

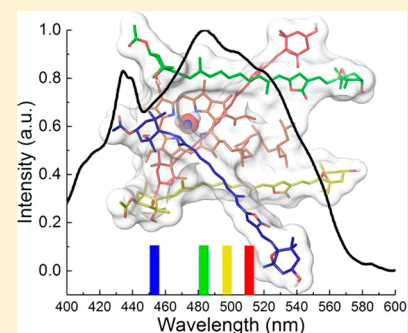
Light Harvesting by Equally Contributing Mechanisms in a Photosynthetic Antenna Protein

Matthew J. Guberman-Pfeffer, Jordan A. Greco,^{1b} Robert R. Birge, Harry A. Frank, and José A. Gascón*^{1b}

Department of Chemistry, University of Connecticut, Storrs, Connecticut 06269-3060, United States

S Supporting Information

ABSTRACT: We report supramolecular quantum mechanics/molecular mechanics simulations on the peridinin–chlorophyll *a* protein (PCP) complex from the causative algal species of red tides. These calculations reproduce for the first time quantitatively the distinct peridinin absorptions, identify multichromophoric molecular excitations, and elucidate the mechanisms regulating the strongly allowed S_0 ($1^1A_g^-$) \rightarrow S_2 ($1^1B_u^+$) absorptions of the bound peridinins that span a 58 nm spectral range in the region of maximal solar irradiance. We discovered that protein binding site-imposed conformations, local electrostatics, and electronic coupling contribute equally to the spectral inhomogeneity. Electronic coupling causes coherent excitations among the densely packed pigments. Complementary pairing of tuning mechanisms is the result of a competition between pigment–pigment and pigment–environment interactions. We found that the aqueous solvent works in concert with the charge distribution of PCP to produce a strong correlation between peridinin spectral bathochromism and the local dielectric environment.



Inspiration and insights for the rational design of artificial photosynthetic devices to meet growing energy demands will benefit from a fundamental understanding of light harvesting strategies employed by natural antenna complexes. An exceptionally efficient antenna complex is the peripheral, water-soluble peridinin–chlorophyll *a* protein (PCP) from photosynthetic marine algae dinoflagellates. PCP collects solar energy over the blue–green spectral region of maximal solar irradiance with >90% efficiency.¹ To realize this superlative functionality, the main form of PCP from the species *Amphidinium carterae* employs the highly substituted C_{37} nor-carotenoid peridinin (Per, Figure 1a) and possesses a unique 4:1 carotenoid-to-chlorophyll *a* stoichiometric ratio in the N- and C-terminal domains of the protein complex (Figure 1b).² In this Letter, we focus on the properties of the reconstituted, recombinant PCP complex, which is a C_2 -symmetric homodimer of the N-terminal domain from the wild-type protein.³

Peridinin features a central heptene chromophore that is conjugated to an allene and contains a butenolide. Both of these exceedingly rare functionalities play a fundamental role in shaping the photophysical response of the chromophore to the properties of the environment.^{4,5}

The spectroscopy of Per that is relevant for the primary absorption event of photosynthesis concerns a strongly allowed excitation from the ground to second excited state (S_0 ($1^1A_g^-$) \rightarrow S_2 ($1^1B_u^+$))⁶ because absorption into S_1 ($2^1A_g^-$) is forbidden by symmetry selection rules. In analogy to a rigorously C_{2v} -symmetric polyene, the S_0 , S_1 , and S_2 states are respectively designated “ $1^1A_g^-$ ”, “ $2^1A_g^-$ ”, and “ $1^1B_u^+$ ”, where the quotation marks emphasize that the designations are approximate. For simplicity and clarity, we will not include quotes around the symmetry labels elsewhere.

The $S_0 \rightarrow S_2$ absorption maximum is sensitive to conformational flexibility, as well as to the polarity, proticity, and polarizability of the environment.⁷ Relative to the $S_0 \rightarrow S_2$ absorption maximum of Per in *n*-hexane, ($\epsilon = 1.89$, $n = 1.38$), the change in solvent polarizability to carbon disulfide ($\epsilon = 2.64$, $n = 1.63$) or polarity to acetonitrile ($\epsilon = 37.5$, $n = 1.34$) only induces a 16–28 nm bathochromic shift.⁷ However, the four Pers bound within a functional domain of PCP (Figure 1b) are known to absorb over a 58 nm range (Figure 1c), with distinct absorption maxima at 453, 483, 497, and 511 nm.³

Theoretical studies have failed to fully reproduce or rationalize the Per spectral inhomogeneity.^{8–12} Only the most red-shifted spectral feature has been assigned experimentally to a specific Per (Per614, Figure 1c),³ and the appropriateness of this 1:1 correspondence between a structure and spectral signature of the PCP-bound Pers has recently been challenged by the detection of a quantum coherent light harvesting mechanism in PCP.^{13,14} Furthermore, it is poorly understood how binding site-selected conformations, chromophore electronic coupling, and the heterogeneous dielectric environment of PCP work in concert to tune the absorption of Per over an optimal spectral range for solar energy capture.

In an effort to address these fundamental questions, we report supramolecular quantum mechanics/molecular mechanics (QM/MM) simulations that tracked the evolution of the $S_0 \rightarrow S_2$ absorption maximum from free Per in vacuum to each of the PCP-bound Pers, as various effects were gradually introduced. First, Per in vacuum assumed the four distinct

Received: December 4, 2017

Accepted: January 16, 2018

Published: January 16, 2018

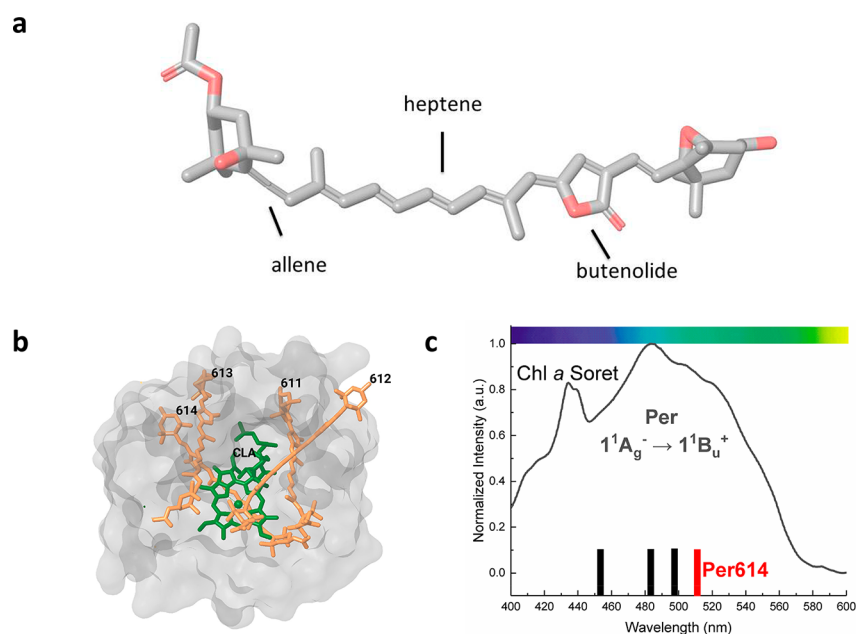


Figure 1. (a) Chemical structure of Per. (b) View of a cofactor cluster inside of the PCP complex consisting of four bound Per molecules and one chlorophyll *a* (Chl *a*) encapsulated by the van der Waals surface of the protein. The lipid digalactosyl diacylglycerol is omitted for clarity. (c) Absorption spectrum of the PCP complex with the S_0 ($1^1A_g^-$) \rightarrow S_2 ($1^1B_u^+$) absorption transition maxima identified from spectral reconstruction in ref 3, indicated with vertical bars. Only one of these spectral signatures has been experimentally attributed to a specific Per structure (Per614), shown in the left figure.

binding site-selected conformations found in PCP. These four conformers were then transferred into the electrostatic environment of PCP, mediated by an aqueous dielectric, to simulate the native environment of the water-soluble complex. Finally, the Pers and Chl *a* of a cofactor cluster within PCP were electronically coupled. The result of the hypothetical progression is shown in Figure 2a and serves as a theoretical bridge between the experimental $S_0 \rightarrow S_2$ absorption maximum of Per in *n*-hexane at the far left and each Per in PCP from spectral reconstruction at the far right. Because the simulated absorption of Per in vacuum and *n*-hexane ($\epsilon = 1$ versus 1.89) only differs by 2 nm, all calculations on the isolated Pers were done in vacuum. The final simulation in the sequence, which achieves quantitative agreement with experiment, features the most sophisticated (fully QM) treatment of pigment–pigment interactions in a domain of PCP to date and stands as a unique instance for the use of implicit solvent in a large-scale multichromophoric QM/MM simulation. Remarkably, the inclusion of an aqueous dielectric will be shown to significantly shape the electrostatic influence of the Per binding sites. In the figure, each simulated absorption wavelength is color-coded to the specific Per that exclusively or predominately carries the excitation.

Figure 2a indicates that the binding sites in PCP mechanically distort the chromophores to break the degeneracy and establish an energetic ranking of the peridinin spectral forms. The simulated $S_0 \rightarrow S_2$ absorption maxima of the conformationally distorted Pers from PCP, isolated in vacuum, are distributed over a 19 nm range. This represents a fraction of the 53 nm spread predicted for the same conformers electronically coupled within the antenna complex, which is in excellent agreement with the 58 nm spread observed experimentally. Distortions red shift the $S_0 \rightarrow S_2$ absorptions of all of the Pers to different extents, except for Per612, which is blue shifted, relative to the fully optimized Per in vacuum. This

is the first assessment of the conformation-induced spectral differentiation achieved in PCP, and the effect is found to be an important contributor to spectral tuning. Sequential addition, in Figure 2a, of the electrostatic environment of the complex mediated by an aqueous dielectric and chromophore electronic coupling broadens the spectral range by an additional 16–18 nm. By “Electrostatic Environment” we mean that each Per was taken separately into the QM region and interacted with the static charge distributions of the other cofactors (the Pers, Chl *a*, and lipid of each monomer), the homodimeric protein, as well as the solvent. The energetic ordering of the Pers is preserved with the exception that Per614 becomes the longest-wavelength absorber, in agreement with experiment.³ In the “Electronic Coupling” stage, the four Pers and Chl *a* (in the M chain of the homodimer) were included in the QM region, effectively adding polarization and delocalization effects in the ground and excited states (i.e., excitonic coupling).

On the basis of the partitioning of effects in Figure 2a, binding site-imposed steric constraints, electrostatic influences, and electronic coupling among densely packed chromophores each contribute 16–19 nm or $\sim 33\%$ to the overall spectral inhomogeneity.

To understand the interplay of interactions between pigments and the interactions of the pigments with the surrounding environment, Figure 2b compares the $S_0 \rightarrow S_2$ absorption maxima for the distorted Pers in vacuum and PCP with different extents of interpigment interaction. The left panel tracks the evolution in the absorption maxima as the isolated and distorted Pers from PCP in vacuum were assembled into the same chromophore cluster found in the antenna complex and electronically coupled. The right panel tracks an analogous evolution under the influence of the aqueously solvated PCP environment. Within the solvated PCP complex, “Distortion” means that the absorption maximum of each distorted Per was calculated in the absence of the nearby chromophores. In the

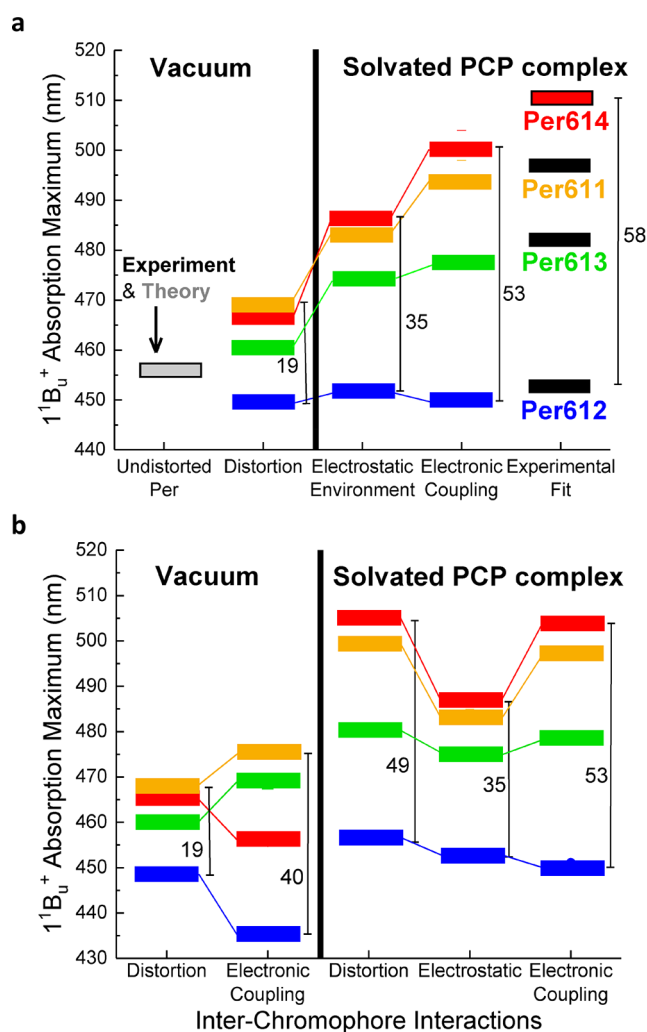


Figure 2. (a) Evolution of the $1^1B_u^+$ absorption maximum of Per as the fully optimized structure in vacuum is transformed into the four protein-bound forms in PCP by adding effects (distortion, electrostatic environment, and electronic coupling). The experimental Per wavelengths are from refs 3 and 7. All predicted transition energies were blue shifted by 0.11 eV (~ 23 nm) so that the predicted wavelength for fully optimized Per in vacuum matched the experimental absorption maximum in *n*-hexane. (b) S_0 ($1^1A_g^-$) \rightarrow S_2 ($1^1B_u^+$) absorption wavelength variation as a function of differing extents of interchromophore interactions in vacuum and within the solvated PCP complex.

next (“Electrostatic”) stage, the other Pers and Chl *a* of the chromophore assembly were introduced as partial atomic charges to electrostatically influence the absorption of one another. This static description of the pigment–charge interactions was then augmented with mutual polarization and exciton delocalization. Figure 2b indicates that electronic coupling in the absence of the PCP environment would extend the spectral range of the distorted Per by 21 nm and severely blue shift Per614 from being the second longest to second shortest wavelength absorber. Per614 only becomes the red-most absorber when the Pers are in the electrostatic field of the PCP complex, regardless of the presence or nature (electrostatic or electronic coupling) of interpigment interactions. Thus, the role of the environment in establishing Per614 as the longest wavelength absorber is consistent with the finding of Schulte et al.³ that mutation of a single residue (Asp-89 to Leu-

89) blue shifted Per614 by 24 nm, causing this Per to no longer be the red-most absorber. Although qualitatively, such a blue shift is also reproduced by our model after mutating in situ Asp-89 to Leu-89.

The difference between the noninteracting Pers in vacuum and noninteracting Pers in PCP reflects the maximal influence of the antenna complex environment. Introduction of the PCP environment to the noninteracting Pers increases the spectral spread by 30 nm and causes Per614 to be the red-most absorber. The subsequent introduction of electrostatic interactions among the chromophores opposes the maximal influence of the rest of the complex and reduces the spectral broadening by 14 nm. The net result of the expansion and contraction in spectral inhomogeneity due to each pigment interacting with the PCP environment and with one another, respectively, constitutes the 16 nm electrostatic contribution to spectral broadening mentioned above. Mutual polarization and exciton delocalization effects recover essentially all of the spectral spread lost through static pigment–charge interactions. This corrective contribution corresponds to the 17 nm attributed to electronic coupling. Another effect of electronic coupling (Table S1) is a redistribution of predicted oscillator strength.

In summary, steric, electrostatic, and interchromophore electronic interactions realized in the PCP complex complement one another by making nearly equal and additive contributions to the $S_0 \rightarrow S_2$ wavelength variation. However, competing or opposing effects are also operative. The PCP electrostatic environment establishes Per614 as the red-most absorbing spectral form, whereas this Per would be the second or third longest wavelength absorber if conformational distortion and electronic coupling were the only factors. With regard to spectral inhomogeneity, static interactions of the Pers with the PCP environment and with one another, as well as static and delocalized aspects of interpigment interactions, form pairs of opposing effects. Thus, complementary and competing mechanisms regulate the primary absorption event of photosynthesis in PCP. Most importantly, the QM/MM calculation, incorporating all of the tuning mechanisms, captures 90% of the experimental $S_0 \rightarrow S_2$ spectral range and reproduces each of the Per absorption signatures within 11 nm of the wavelengths from spectral reconstruction (Figure 2a).³

Our quantitative model of electronically coupled chromophores in PCP permits the first characterization of the excitons long-suspected from circular dichroism spectra to be present in the antenna complex^{15,16} but only recently inferred by two-dimensional electronic spectroscopy.¹³ Figure 3 depicts the nature of the $1^1B_u^+$ excitons from a natural transition orbital (NTO) perspective. NTOs represent the contributing configurations to an excitation in terms of paired hole and particle orbitals.^{17,18} Because inclusion of Chl *a* at the QM level perturbed the simulated absorption maxima by ≤ 5 nm and for simplicity in visualizing the NTOs, Figure 3 reports the result of only electronically coupling four Pers while modeling Chl *a* and the rest of the protein electrostatically in the MM region. Figure 3 shows that excitations are delocalized over two Pers at the longest and shortest wavelength absorptions and over three Pers at intermediate wavelengths. All of the excitations involve displacement of electron density from the allene to the butenolide of separate Pers (Figure S1). The leading terms for these excitations place at least 50% of the transition on a single Per. If the spectral signatures are assigned on the basis of the leading contributions to the simulated excitations, the

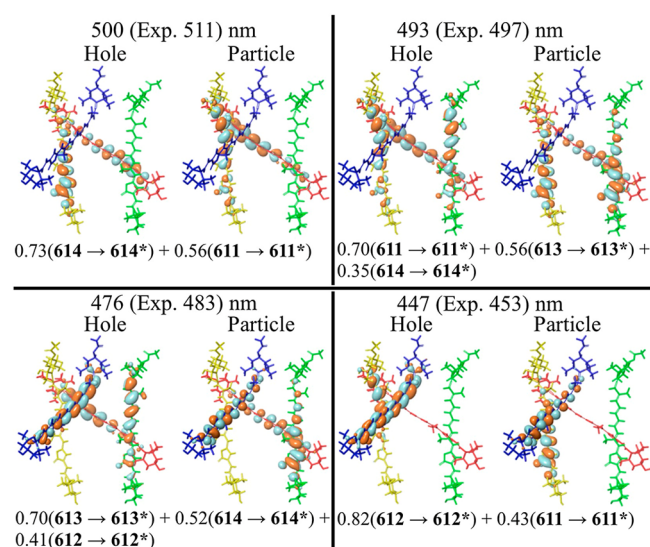


Figure 3. NTO perspective of the $1^1B_u^+$ excitons for a tetramer of Pers within PCP in an aqueous dielectric. The environment for the Pers is omitted for clarity. The largest contributing NTOs comprising $\geq 85\%$ of each excitation are shown with an isosurface of 0.02 au. Pers 611–614 are colored yellow, blue, green, and red, respectively. Absorption wavelengths and a description of the excitons in the basis of hole–particle NTOs localized on individual Pers are provided.

wavelength ordering of the Per spectral forms is Per613 < Per611 < Per614. This result is consistent with the experimental deduction that Per614 is the red-most spectral form,³ confirms the previous theoretical suggestion that Per612 is the bluest absorber,⁹ and completes the interpretative gap between the crystal structure and the congested solution-phase absorption spectrum (Figure 1c).

The energetic ranking of $S_0 \rightarrow S_2$ excitons is established through geometric distortion of the Pers and only minimally refined by other factors (Figure 2a). This conformational spectral effect is attributable to torsional deformations that can be understood by applying the strategy of normal structure decomposition^{19,20} (NSD). The NSD approach decomposes protein-induced cofactor conformations in terms of displacements along vibrational normal modes of a reference structure. The distinct Per conformers are well approximated in terms of the three lowest normal coordinate deformations of a C_s -symmetric Per (Figure 4a). Out-of-plane and in-plane distortions of the PCP-bound Pers on the left reflect contributions from normal coordinate displacements of the reference structure at the right. Figure 4b shows the corresponding spectral shifts for the crystallographic conformations (solid bars), as well as the contributing out-of-plane and in-plane normal modes (vertically and horizontally striped bars, respectively) relative to the predicted $S_0 \rightarrow S_2$ absorption maximum of the C_s -symmetric Per. All of the Pers exhibit standing wave-type distortions. Per613 features the first harmonic of a standing wave, whereas Per611, Per612, and Per614 display the first overtone mode. These conformations resemble the first and third normal modes of the C_s -symmetric Per, respectively. Displacements along either coordinate induce spectral bathochromism. All of the Pers also exhibit an in-plane bowing deformation, which corresponds to a contribution from the second normal mode. Interestingly, Per612 bows in an opposite direction to the other Pers. Displacement of the reference Per along this normal coordinate in the direction

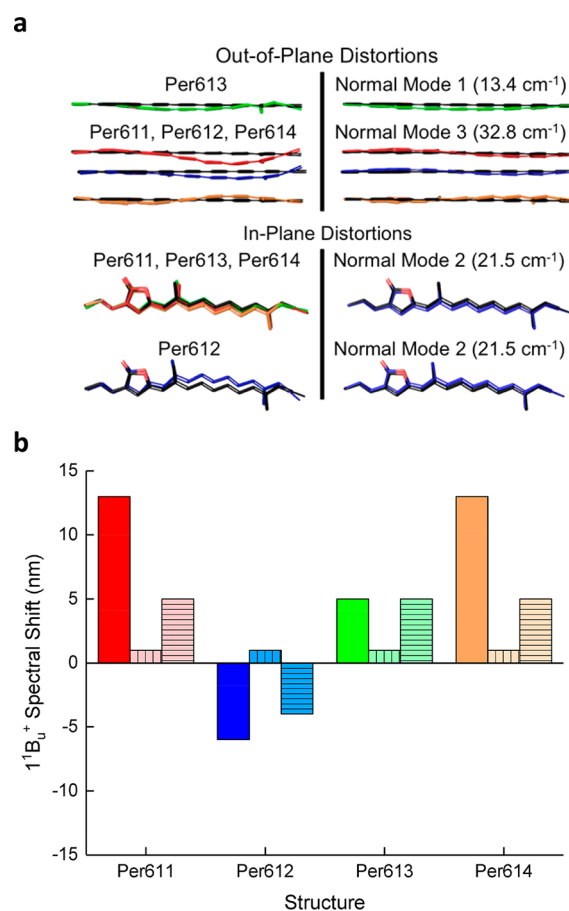


Figure 4. (a) Comparison of crystallographic Per distortions (left panel) to the most prominently contributing normal coordinate deformations (right panel). (b) Spectral shifts for the crystallographic Per conformers (solid bars) and the contributing out-of-plane and in-plane normal coordinate deformations (vertically and horizontally striped bars, respectively) relative to the predicted $1^1B_u^+$ absorption maximum for the C_s -symmetric Per model. For direct comparison with the reference structure, the crystallographic Pers were truncated (terminal rings replaced by hydrogens).

exhibited by Per612 causes a blue shift, whereas bowing in the opposite direction, as in the other Pers, induces a red shift. Thus, we propose that this deformation mode is at least partly responsible for the assignment of Per612 as the bluest spectral form in PCP.

Another important observation is related to the role of solvent. The retention of the conformationally induced ordering of the Per spectral forms from vacuum to PCP (Figure 2a) only holds if the native aqueous environment of the antenna complex is included. If vacuum simulations are performed on the chromophore cluster with or without the rest of the PCP complex, incorrect ordering of the Pers is obtained (Figure S2). These observations suggest a significant spectral role (never assessed in previous literature) for the aqueous dielectric that mediates interchromophore interactions, as well as the anisotropic and highly charged surface of the water-soluble complex. In support of this hypothesis, we find a strong correlation whereby Pers surrounded by more, and primarily hydrophobic, residues within 5 Å absorb at longer wavelengths in the implicitly solvated complex (Figure S2).

We have demonstrated for the first time the precise blend of complementary and competing mechanisms that tune the

absorption of Per in PCP over the entire blue–green spectral region in which solar irradiance is greatest, and where Chl *a* has minimal absorption. Our methods, model, and mechanistic insights can assist the rational design of artificial photosynthetic devices that employ wild-type or mutated PCP antennas, bioinorganic PCP hybrids, or other bioinspired light harvesting systems.

■ COMPUTATIONAL METHODS

A model of the reconstituted PCP complex from the highest-resolution crystal structure available (PDB ID 3IIS; 1.4 Å)³ was prepared. All QM/MM simulations were performed using Qsite²¹ from Schrodinger Inc.²² using the Poisson–Boltzmann finite difference (PBF) method.²³ The B3LYP/LACVP* model chemistry and the OPLSS-AA force field were used for the QM and MM regions, respectively. Vertical excitations were computed at the time-dependent DFT (TD-DFT) level with the Tamm–Dancoff approximation (TDA). This methodology has been successfully applied previously to predict carotenoid spectra.²⁴

■ ASSOCIATED CONTENT

📄 Supporting Information

The Supporting Information is available free of charge on the ACS Publications website at DOI: 10.1021/acs.jpcllett.7b03211.

Details on the computational methods and vacuum versus implicit solvent calculations (PDF)

■ AUTHOR INFORMATION

Corresponding Author

*E-mail: jose.gascon@uconn.edu

ORCID

Jordan A. Greco: 0000-0001-7582-9321

José A. Gascón: 0000-0002-4176-9030

Notes

The authors declare no competing financial interest.

■ ACKNOWLEDGMENTS

Support through NSF Grant CHE-0754580 (J.A. Gascón) and M.G.-P.'s graduate fellowship DGE-1247393 is gratefully acknowledged.

■ REFERENCES

- (1) Carbonera, D.; Di Valentin, M.; Spezia, R.; Mezzetti, A. The unique photophysical properties of the Peridinin-Chlorophyll-*a*-Protein. *Curr. Protein Pept. Sci.* **2014**, *15*, 332–350.
- (2) Hofmann, E.; Wrench, P. M.; Sharples, F. P.; Hiller, R. G.; Welte, W.; Diederichs, K. Structural Basis of Light Harvesting by Carotenoids: Peridinin-Chlorophyll-Protein from Amphidinium carterae. *Science* **1996**, *272*, 1788–1791.
- (3) Schulte, T.; Niedzwiedzki, D. M.; Birge, R. R.; Hiller, R. G.; Polívka, T.; Hofmann, E.; Frank, H. A. Identification of a single peridinin sensing Chl-*a* excitation in reconstituted PCP by crystallography and spectroscopy. *Proc. Natl. Acad. Sci. U. S. A.* **2009**, *106*, 20764–20769.
- (4) Olpp, T.; Brückner, R. Total Synthesis of the Light-Harvesting Carotenoid Peridinin. *Angew. Chem., Int. Ed.* **2006**, *45*, 4023–4027.
- (5) Hoffmann-Röder, A.; Krause, N. Synthesis and properties of allenic natural products and pharmaceuticals. *Angew. Chem., Int. Ed.* **2004**, *43*, 1196–1216.
- (6) Hudson, B. S.; Kohler, B. E. A low-lying weak transition in the polyene α , ω -diphenyloctatetraene. *Chem. Phys. Lett.* **1972**, *14*, 299–304.

- (7) Bautista, J. A.; Connors, R. E.; Raju, B. B.; Hiller, R. G.; Sharples, F. P.; Gosztola, D.; Wasielewski, M. R.; Frank, H. A. Excited state properties of peridinin: observation of a solvent dependence of the lowest excited singlet state lifetime and spectral behavior unique among carotenoids. *J. Phys. Chem. B* **1999**, *103*, 8751–8758.

- (8) Carbonera, D.; Giacometti, G.; Segre, U.; Hofmann, E.; Hiller, R. G. Structure-based calculations of the optical spectra of the light-harvesting peridinin–chlorophyll–protein complexes from Amphidinium carterae and Heterocapsa pygmaea. *J. Phys. Chem. B* **1999**, *103*, 6349–6356.

- (9) Shima, S.; Ilagan, R. P.; Gillespie, N.; Sommer, B. J.; Hiller, R. G.; Sharples, F. P.; Frank, H. A.; Birge, R. R. Two-photon and fluorescence spectroscopy and the effect of environment on the photochemical properties of peridinin in solution and in the peridinin-chlorophyll-protein from Amphidinium carterae. *J. Phys. Chem. A* **2003**, *107*, 8052–8066.

- (10) Bovi, D.; Mezzetti, A.; Vuilleumier, R.; Gageot, M.-P.; Chazallon, B.; Spezia, R.; Guidoni, L. Environmental effects on vibrational properties of carotenoids: experiments and calculations on peridinin. *Phys. Chem. Chem. Phys.* **2011**, *13*, 20954–20964.

- (11) Bricker, W. P.; Lo, C. S. Excitation Energy Transfer in the Peridinin-Chlorophyll *a*-Protein Complex Modeled Using Configuration Interaction. *J. Phys. Chem. B* **2014**, *118*, 9141–9154.

- (12) Bricker, W. P.; Lo, C. S. Efficient Pathways of Excitation Energy Transfer from Delocalized S₂ Excitons in the Peridinin–Chlorophyll *a*–Protein Complex. *J. Phys. Chem. B* **2015**, *119*, 5755–5764.

- (13) Roscioli, J. D.; Ghosh, S.; LaFountain, A. M.; Frank, H. A.; Beck, W. F. Quantum Coherent Excitation Energy Transfer by Carotenoids in Photosynthetic Light Harvesting. *J. Phys. Chem. Lett.* **2017**, *8*, 5141–5147.

- (14) Ghosh, S.; Bishop, M. M.; Roscioli, J. D.; LaFountain, A. M.; Frank, H. A.; Beck, W. F. Excitation Energy Transfer by Coherent and Incoherent Mechanisms in the Peridinin–Chlorophyll *a* Protein. *J. Phys. Chem. Lett.* **2017**, *8*, 463–469.

- (15) Song, P.-S.; Koka, P.; Prezelin, B. B.; Haxo, F. T. Molecular topology of the photosynthetic light-harvesting pigment complex, peridinin-chlorophyll *a*-protein, from marine dinoflagellates. *Biochemistry* **1976**, *15*, 4422–4427.

- (16) Pilch, M.; Pawlikowski, M. Circular dichroism (CD) study of peridinin–chlorophyll *a* protein (PCP) complexes from marine dinoflagellate algae The tetramer approach. *J. Chem. Soc., Faraday Trans.* **1998**, *94*, 227–232.

- (17) Dreuw, A.; Head-Gordon, M. Single-reference ab initio methods for the calculation of excited states of large molecules. *Chem. Rev.* **2005**, *105*, 4009–4037.

- (18) Martin, R. L. Natural transition orbitals. *J. Chem. Phys.* **2003**, *118*, 4775–4777.

- (19) Jentzen, W.; Song, X.-Z.; Shelnut, J. A. Structural characterization of synthetic and protein-bound porphyrins in terms of the lowest-frequency normal coordinates of the macrocycle. *J. Phys. Chem. B* **1997**, *101*, 1684–1699.

- (20) Senge, M. O.; MacGowan, S. A.; O'Brien, J. M. Conformational control of cofactors in nature—the influence of protein-induced macrocycle distortion on the biological function of tetrapyrroles. *Chem. Commun.* **2015**, *51*, 17031–17063.

- (21) Murphy, R. B.; Philipp, D. M.; Friesner, R. A. A mixed quantum mechanics/molecular mechanics (QM/MM) method for large-scale modeling of chemistry in protein environments. *J. Comput. Chem.* **2000**, *21*, 1442–1457.

- (22) Schrodinger Inc., release 2017-1; New York, 2017.

- (23) Tannor, D. J.; Marten, B.; Murphy, R.; Friesner, R. A.; Sitkoff, D.; Nicholls, A.; Honig, B.; Ringnalda, M.; Goddard, W. A., III Accurate first principles calculation of molecular charge distributions and solvation energies from ab initio quantum mechanics and continuum dielectric theory. *J. Am. Chem. Soc.* **1994**, *116*, 11875–11882.

- (24) Andreussi, O.; Knecht, S.; Marian, C. M.; Kongsted, J.; Mennucci, B. Carotenoids and Light-Harvesting: From DFT/MRCI to

the Tamm–Dancoff Approximation. *J. Chem. Theory Comput.* **2015**, *11*, 655–666.